Backstepping Control of the Toroidal Plasma Current Profile in the DIII-D Tokamak

Mark D. Boyer, Justin Barton, Eugenio Schuster, Michael L. Walker, Tim C. Luce, John R. Ferron, Ben G. Penaflor, Robert D. Johnson, and David A. Humphreys

***Abstract*— One of the most promising devices for realizing power production through nuclear fusion is the tokamak. To maximize performance, it is preferable that tokamak reactors achieve advanced operating scenarios characterized by good plasma confinement, improved magnetohydrodynamic stability, and a largely noninductively driven plasma current. Such scenarios could enable steady-state reactor operation with high fusion gain, the ratio of produced fusion power to the external power provided through the plasma boundary. For certain advanced scenarios, control of the spatial profile of the plasma current will be essential. The complexity of the current profile dynamics, arising due to nonlinearities and couplings with many other plasma parameters, motivates the use of model-based control algorithms that can account for the system dynamics. A first-principles-driven, control-oriented model of the current profile evolution in low-confinement mode (L-mode) discharges in the DIII-D tokamak is employed to address the problem of regulating the current profile evolution around desired trajectories. In the primarily inductive L-mode discharges considered in this paper, the boundary condition, which is dependent on the total plasma current, has the largest influence on the current profile dynamics, motivating the design of a boundary feedback control law to improve the system performance. The backstepping control design technique provides a systematic method to obtain a boundary feedback law through the transformation of a spatially discretized version of the original system into an asymptotically stable target system with desirable properties. Through a nonlinear transformation of the available physical actuators, the resulting control scheme produces references for the total plasma current, total power, and line averaged density, which are tracked by existing dedicated control loops. Adaptiveness is added to the control scheme to improve upon the backstepping controller's disturbance rejection and tracking capability. Prior to experimental testing, a Simserver simulation was carried out to study the controller's performance and ensure proper implementation in the DIII-D Plasma Control System. An experimental test was performed on DIII-D to test the ability of the controller to reject input disturbances and perturbations in initial conditions and to demonstrate the feasibility of the proposed control approach.**

***Index Terms*— Current profile control, nonlinear PDE control, plasma control, tokamaks.**

I. Introduction

NUCLEAR fusion, the process by which two light nuclei combine to form a heavier nucleus, is accompanied by a conversion of a small amount of mass into a large amount of energy, making it a potential means for producing electrical power. The most likely fusion fuels are plentiful: deuterium can be extracted from sea water and tritium can be bred from lithium. In addition, there is no emission of green house gases or air pollution, and, unlike nuclear fission, there is no risk of a runaway nuclear reaction, and no generation of high-level nuclear waste or weapon-grade material. These advantages make fusion an attractive alternative to the use of fossil fuels or nuclear fission for power production. However, nuclear fusion is extremely challenging from both scientific and technical perspectives. Extremely high temperatures (on the order of 100 million degrees) are required for fusion reactions to occur frequently enough to make a reactor economically viable as a source of energy. At these temperatures, the fuel mixture becomes a plasma. In a plasma, the fourth state of matter, the electrons are stripped from the nuclei of the atoms, creating an ionized gas of independent negatively and positively charged particles. Importantly, these charged particles can conduct electricity and interact with magnetic fields. These characteristics can be exploited to both heat and confine plasmas.

Due to the Lorentz force, charged particles will travel in a helical path around the field lines of a uniform applied magnetic field. To create a closed geometry for confining and controlling a fusion plasma, the tokamak [1], one of the most promising devices, closes and twists the applied magnetic field lines into a helical structure, trapping the ionized gas inside a toroidal vessel and creating a magnetohydrodynamic equilibrium [2]. A schematic of the coils and the magnetic fields in a tokamak is shown in Fig. 1. The D-shaped toroidal field (TF) coils (shown in blue) generate the toroidal component of the magnetic field (also shown in blue). The plasma electric current (shown in green) is mainly generated through transformer action in which both the inner poloidal field coils (also shown in green) and outer poloidal field coils (shown in gray) act as the primary coil and the plasma itself acts as the secondary coil. The combination of the

Manuscript received September 20, 2013; accepted November 30, 2013. Manuscript received in final form December 20, 2013. Date of publication February 4, 2014; date of current version July 24, 2014. This work was supported in part by the National Science Foundation CAREER Award Program under Grant ECCS-0645086 and in part by the U.S. Department of Energy under Grant DE-FG02-09ER55064 and Grant DE-FC02-04ER54698. Recommended by Associate Editor M. Mattei.

M. D. Boyer, J. Barton, and E. Schuster are with the Department of Mechanical Engineering and Mechanics, Lehigh University, Bethlehem, PA 18015 USA (e-mail: m.dan.boyer@lehigh.edu; justin.barton@lehigh.edu; schuster@lehigh.edu).

M. L. Walker, T. C. Luce, J. R. Ferron, B. G. Penaflor, R. D. Johnson, and D. A. Humphreys are with General Atomics, San Diego, CA 92121 USA (e-mail: walker@fusion.gat.com; luce@fusion.gat.com; ferron@fusion.gat.com; penaflor@fusion.gat.com; johnsonb@fusion.gat.com; humphreys@fusion.gat.com).

Color versions of one or more of the figures in this paper are available online at http://ieeexplore.ieee.org.

Digital Object Identifier 10.1109/TCST.2013.2296493

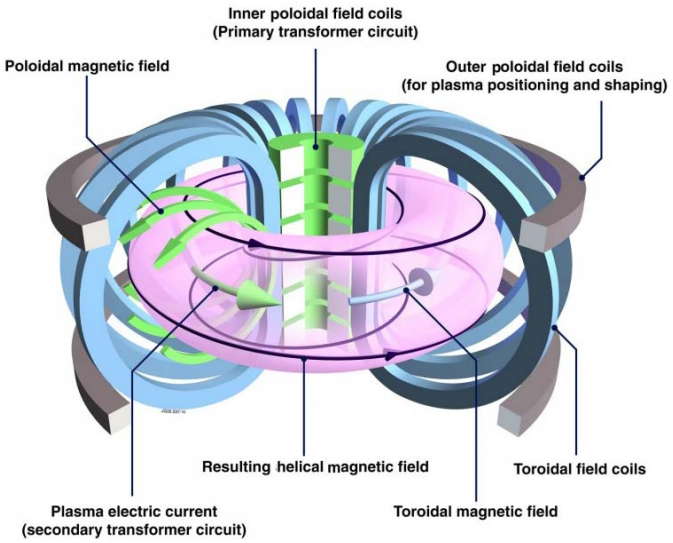

Fig. 1. Diagram of the coils and magnetic fields in a tokamak. (Image source: EFDA.)

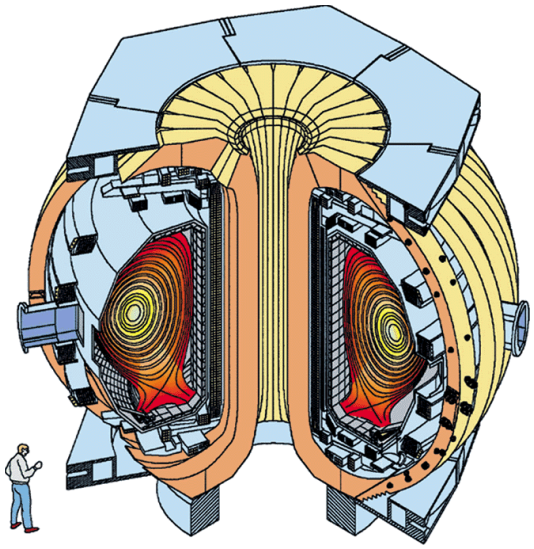

Fig. 2. Illustration of the DIII-D tokamak. The TF coils (cream colored) and poloidal field coils (light blue) produce the magnetic field that confines the plasma. The cross section of the plasma within the machine is represented by a set of magnetic flux contours. (Image source: General Atomics Fusion Education Outreach.)

toroidal and poloidal components results in a helical magnetic field line around the tokamak (shown in black). The poloidal field coils are also used to position and shape the plasma.

Over the past few decades, numerous experimental tokamaks have made a great deal of progress in understanding the physics of tokamak plasmas. ITER, which is the next experimental step for tokamak fusion research, will attempt to be the first device to achieve a burning plasma (one in which a majority of the heat needed to sustain the plasma comes from fusion reactions) and to show the scientific feasibility of a commercial nuclear fusion power plant. Before ITER and future nuclear fusion power plants can begin operation, several challenging control problems must be addressed. An overview of these control problems can be found in [3] and [4].

Among the major challenges is to achieve scenarios in which a tokamak can operate with sufficiently long plasma discharges. As explained before, the plasma current needed for confinement is primarily achieved through induction in most existing tokamaks. Plasma current generated through induction cannot be sustained for extended periods of time and steady-state tokamak operation will require the plasma current to be driven entirely by noninductive means. It has been demonstrated that setting up a suitable spatial distribution of the toroidal plasma current is key to enabling certain advanced operating scenarios characterized by high fusion gain and noninductive sustainment of plasma current that could allow for steady-state operation (see [5]). Typically, the spatial distribution of toroidal current is approximated as a 1-D radial profile by assuming axisymmetry in the toroidal coordinate and by averaging quantities over the poloidal magnetic flux surfaces, a set of nested surfaces of constant poloidal magnetic flux, as shown in the cutaway view of the plasma inside the DIII-D tokamak in Fig. 2. The poloidal magnetic flux ψ at point P is the total flux through the horizontal surface S bounded by the toroidal ring passing through P, i.e., $\psi = \int B_{\text{pol}} dS$, where B_{pol} denotes the poloidal component of the magnetic field. As part of the effort to identify and achieve suitable profiles for advanced operating scenarios, active control of the current profile or the safety factor profile, q, a related quantity defined as the number of times a magnetic field line goes around the machine toroidal for each time it goes around poloidally, has become an area of extensive research.

A. Prior Work

Most experiments in this area have thus far focused on the real-time feedback control of scalar parameters characterizing some aspect of the current profile. In [6], feedback control of $q(0, t)$, the safety factor at the magnetic axis of the plasma, or $q_{\min}(t)$, the minimum value of the safety factor profile, was achieved by modifying either electron cyclotron heating (ECH) or neutral beam injection (NBI) on DIII-D. In [7], lower hybrid current drive (LHCD) was used to control the internal inductance parameter, $l_i(t)$, a measure of the current profile shape, on Tore Supra. Both experiments used simple nonmodel-based proportional control laws to modify single scalar parameters describing some characteristic of the current profile. Nonmodel-based approaches to real-time control of the current profile were also studied in [8]–[10].

Though nonmodel-based techniques have had some success in manipulating single scalar outputs, like $l_i(t)$ or $q_{\min}(t)$, it will be critical to control the shape of the entire current profile to achieve certain advanced tokamak operating scenarios. The strong nonlinear coupling between magnetic and kinetic profiles and the high dimensionality of this type of distributed control problem motivate the use of model-based techniques that can exploit knowledge of the dynamic response of the system to the available actuators within the controller design. Compared with nonmodel-based approaches, model-based designs can achieve high levels of performance without requiring significant amounts of experimental time for trial-and-error tuning. Work on dynamic modeling of the current profile evolution has focused on either generating

models from experimental data or creating models motivated by a first-principles description of the system.

Data-driven models have recently been used to design controllers for simultaneous regulation of magnetic and kinetic plasma profiles around desired references during the flattop phase of a plasma discharge at JET [11]–[13], JT-60U, and DIII-D [14]–[16]. In this approach, system identification techniques were used to develop linear dynamic models of the plasma profile response to various actuators based on data gathered during dedicated experiments. Because the resulting models are linear, they are only valid close to the reference scenario used for identification. As a result, controllers based on these models may perform poorly if the system states move far from their respective reference values. Additional dedicated system identification experiments must be carried out to apply this approach to new devices or to different operating scenarios.

By designing controllers using a first-principles description of the current profile dynamics, the issues associated with identified models can be largely avoided. In practice, it is typically necessary to simplify or approximate the first-principles description by closing the model equations with empirical expressions to facilitate control design. If these approximations are made carefully, the advantages of a first-principles model-based approach to control design can be largely retained while the complexity of the model and control design can be greatly reduced. To distinguish this simplified physics-based modeling approach from those based purely on first-principles or those identified entirely from empirical data, we refer to the resulting simplified models as first-principles-driven, and control-oriented models. Use of a first-principles-driven model allows the control design to incorporate the nonlinear coupling of the plasma parameters, potentially enabling improved closed-loop performance and allowing for operation over a wider range of conditions when compared with control schemes based on linear data-driven models. In addition, first-principles driven controllers have the potential to be adapted to different scenarios or devices without significant changes to the structure of the control law and while avoiding the need for dedicated model identification experiments. Such models of the evolution of the plasma magnetic flux have recently been developed in [17]–[19]. In [20] and [21], the model developed in [17] was used to calculate optimal feedforward actuator trajectories for achieving a desired safety factor profile, using extremum-seeking and nonlinear programming approaches, respectively. Some recent work on first-principles-driven feedback control designs have been presented in [22]–[28]. In these results, robust, optimal, and sliding mode-based feedback controllers were developed and tested in simulations.

B. Results of This Paper

In this paper, we design a first-principles driven, model based, current profile, feedback-control algorithm for L-mode discharges on DIII-D. This algorithm is designed to be combined with feedforward actuator trajectories that can be calculated offline (see [20] and [21]) or extracted from previous experimental discharges. The model-based feedback control law enables the actuator trajectories to be adjusted in real-time in order to reproduce profile evolutions achieved in previous experiments or simulations despite perturbed initial conditions or other disturbances. We design the controller to track a reference trajectory of the poloidal flux gradient profile θ, a quantity inversely related to the safety factor profile. Because the plasma current in the L-mode discharges studied in this paper is primarily inductively driven, the most effective means of controlling the current profile is through the boundary condition, which can be actuated through modulation of the total plasma current. This defines a boundary-control problem for a system whose dynamics is described by a partial differential equation (PDE). To tackle this problem, a boundary feedback control law is designed in this paper by discretizing in space the PDE describing the evolution of θ in L-mode discharges on DIII-D using a finite difference method and by following a backstepping procedure to obtain a transformation from the original system into an asymptotically stable target system. The feedback term from the resulting control law is added to the feedforward input trajectories and, through a nonlinear transformation, references are obtained for the plasma current, noninductive power, and line-averaged density. These references are then sent to existing dedicated controllers for the individual physical quantities.

Backstepping provides a systematic method for designing boundary-control laws for PDE systems where actuation is applied at the boundary and must be propagated through spatial dynamics. The method achieves stability and performance improvement by using a feedback transformation to eliminate undesirable terms or to add missing terms, while leaving the system in a physically relevant and familiar form. This enables physical intuition to be used to shape the closed-loop response. The control gain is obtained by using a simple recursive numerical calculation, which avoids the need to solve high-dimensional Riccati equations. Furthermore, the approach can be used to handle time-varying model parameters and nonlinear terms, which will be exploited in future work to, for example, account for changes in plasma shape or the presence of significant bootstrap current drive in high-confinement (H-mode) discharges. Boundary actuation will also be the primary actuator for controlling current profile formation during the ramp-up and early flattop phases of H-mode discharges. In the flattop phase of H-mode discharges, however, interior actuation through noninductive current drives become more effective and its use as feedback control actuators could potentially improve closed-loop performance. Since backstepping control design offers a systematic approach to the integration of boundary and interior control [29], the design of a backstepping boundary feedback control law in this paper is, therefore, not only relevant for L-mode plasmas but also an important step toward the design of a comprehensive current profile control strategy for H-mode discharges.

In this paper, we have taken a discretize then design approach to designing the backstepping controller [30], rather than the design then discretize approach taken in [31]. This results in a simple recursive formula for an approximation to the infinite dimensional gain kernel that would be derived using the latter approach. The approximation, which holds for

any finite spatial grid, can be improved through the use of a fine grid. However, it has been seen that a controller designed on a coarse grid (using a small number of measurements of the profile) can achieve satisfactory closed-loop response when tested in simulations (with a much finer grid used for simulating the PDE model) and experiments. We note that the discretize then design backstepping technique has been applied to open-loop unstable nonlinear chemical reactions in [32] and [33] and has been applied to other tokamak control problems, specifically the problem of kinetic profile control, in [34]–[36].

Numerical simulations show that improved performance is achieved through the use of the backstepping control scheme. However, because the resulting control law only uses proportional feedback, the controller's ability to reject disturbances is limited. To overcome this limitation, we augment the backstepping control law with an adaptive law that effectively adds integral action to the closed-loop system. The resulting control scheme takes the form of a multiple input single output proportional–integral controller coupled with nonlinear input transformations, with spatially varying gains derived through the use of a backstepping procedure and tuned through the choice of design parameters in the target system. Simulation results show that this approach can greatly improve the disturbance rejection capabilities of the closed-loop system. As a part of this paper, a general framework for implementing real-time feedforward control of magnetic and kinetic plasma profiles was implemented in the DIII-D Plasma Control System (PCS). The framework was used to experimentally test the control design and demonstrate the feasibility of the proposed current profile control scheme. These results are part of the first experimental campaign to perform model-based feedback control of the current profile using a first-principles-driven modeling approach and represent the first experimental implementation of a backstepping boundary control law in a tokamak. Results of our other approaches to first-principles-driven model-based feedback control design that were tested during the same campaign can be found in [37] and [38].

C. Organization

This paper is organized as follows. In Section II, a PDE model for the current profile evolution is introduced. The control objective is discussed in Section III. In Section IV, a backstepping feedback control law is presented and the stability of the target system is shown. The addition of an adaptive law to improve upon disturbance rejection is also discussed. The real-time control algorithm and the simulation framework are described in Section V. The feedback control laws are studied in simulations and experimentally tested in Sections VI and VII, respectively. Finally, conclusions and future work are stated in Section VIII.

II. Current Profile Evolution Model

We begin by taking ρ as a coordinate indexing the magnetic surfaces within a poloidal cross section of the tokamak plasma. We choose the mean effective radius of the magnetic surface as the variable ρ, i.e., $\pi B_{\phi,0}\rho^2 = \Phi$, where Φ is the toroidal magnetic flux and $B_{\phi,0}$ is the reference magnetic field at the geometric major radius R_0 of the tokamak. By normalizing the quantity by ρ_b, the mean effective minor radius of the last closed magnetic surface, we obtain the coordinate $\hat{\rho} = \rho/\rho_b$. Fig. 3 illustrates the coordinate system. The safety factor, a quantity related to the toroidal current density, is given by $q(\rho, t) = -d\Phi/d\Psi(\rho, t)$, where Ψ is the poloidal magnetic flux. By noting the constant relationship between ρ and Φ, i.e., $\pi B_{\phi,0}\rho^2 = \Phi$, and the definition of ρ_b, this can be written as

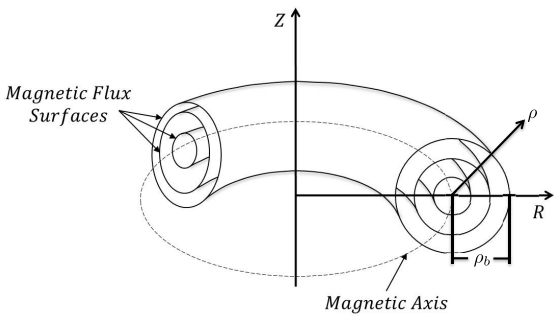

Fig. 3. Illustration of the coordinates used in the current profile model.

$$q\left(\hat{\rho}, t\right) = -\frac{B_{\phi,0}\rho_b^2\hat{\rho}}{\partial\psi/\partial\hat{\rho}} \tag{1}$$

where ψ is the poloidal stream function ($\Psi = 2\pi\psi$). Since the safety factor depends inversely on the spatial derivative of the poloidal flux, we define

$$\theta\left(\hat{\rho}, t\right) = \frac{\partial\psi}{\partial\hat{\rho}}\left(\hat{\rho}, t\right) \tag{2}$$

and take this quantity as the variable of interest to be controlled. This choice is motivated by the straightforward derivation of a PDE for the dynamics of $\theta\left(\hat{\rho}, t\right)$, and is possible because any target for $q\left(\hat{\rho}, t\right)$ can be uniquely related to a target for $\theta\left(\hat{\rho}, t\right)$.

To obtain a PDE describing the evolution of $\theta\left(\hat{\rho}, t\right)$, we start from the well-known magnetic diffusion equation [17], [39], [40], which describes the poloidal magnetic flux evolution. This equation is given by

$$\frac{\partial\psi}{\partial t} = \frac{\eta(T_e)}{\mu_0\rho_b^2\hat{F}^2}\frac{1}{\hat{\rho}}\frac{\partial}{\partial\hat{\rho}}\left(\hat{\rho}\hat{F}\hat{G}\hat{H}\frac{\partial\psi}{\partial\hat{\rho}}\right) + R_0\hat{H}\eta(T_e)\frac{\langle\bar{j}_{\mathrm{NI}}\cdot\bar{B}\rangle}{B_{\phi,0}} \tag{3}$$

where ψ represents the poloidal magnetic flux, t is time, and η is the plasma resistivity, which is dependent on the electron temperature, T_e, μ_0 is the vacuum permeability, $\bar{j}_{\mathrm{NI}}$ is the noninductive current density from neutral beam injection (NBI), $\bar{B}$ is the toroidal magnetic field, and $\langle\rangle$ denotes the flux-surface average of a quantity. $\hat{F}$, $\hat{G}$, and $\hat{H}$ are spatially varying geometric factors of the DIII-D tokamak that are described in [17]. These factors vary in time as the plasma shape evolves (especially during the ramp-up phase). However, they are considered to be constant in this model. While the proposed control method could accommodate time-varying model parameters, initial experimental results indicate that it

may not be necessary to include this increased complexity in the model for the purposes of control design. The boundary conditions are given by

$$\left.\frac{\partial \psi}{\partial \hat{\rho}}\right|_{\hat{\rho}=0} = 0, \quad \left.\frac{\partial \psi}{\partial \hat{\rho}}\right|_{\hat{\rho}=1} = -\frac{\mu_0}{2\pi}\frac{R_0}{\hat{G}\big|_{\hat{\rho}=1}\hat{H}\big|_{\hat{\rho}=1}} I(t) \tag{4}$$

where $I(t)$ is the total plasma current.

Based on experimental observations of the ramp-up phase in L-mode discharges in DIII-D, simplified scenario-oriented empirical models for the electron temperature, noninductive current density, and plasma resistivity were identified [17]. The temperature and noninductive current drive terms are considered to have fixed spatial profiles with time-varying magnitudes that scale with the values of physical actuators. The model for the electron temperature is given by

$$T_e\left(\hat{\rho}, t\right) = k_{T_e} T_e^{\text{profile}}\left(\hat{\rho}\right) \frac{I(t)\sqrt{P_{\text{tot}}(t)}}{\bar{n}(t)} \tag{5}$$

where k_{T_e} is a constant, $T_e^{\text{profile}}\left(\hat{\rho}\right)$ is a reference profile, $P_{\text{tot}}(t)$ is the total average NBI power, and $\bar{n}(t)$ is the line averaged plasma density. This scaling law can be derived by considering an approximate steady-state energy balance, i.e., $E/\tau_E = P_{\text{tot}}$, where E is the plasma stored energy, and the energy confinement time τ_E is considered to be proportional to $\text{IP}_{\text{tot}}^{-0.5}$, as suggested in [41]. The steady-state solution is used because the energy time-scale is much shorter than the current diffusion time-scale. The model for the noninductive toroidal current density is given by

$$\frac{< \bar{j}_{\text{NI}} \cdot \bar{B} >}{B_{\phi,0}} = k_{\text{NI}} j_{\text{NI}}^{\text{profile}}\left(\hat{\rho}\right) \frac{I(t)^{1/2} P_{\text{tot}}(t)^{5/4}}{\bar{n}(t)^{3/2}} \tag{6}$$

where k_{NI} is a constant and $j_{\text{NI}}^{\text{profile}}\left(\hat{\rho}\right)$ is a reference profile for the noninductive current deposition. This scaling is derived by considering the neutral beam current drive to be proportional to $P_{\text{tot}} T^{0.5} n^{-1}$, which is a suitable approximation of the formula given in [42] for parameters in DIII-D, and substituting the temperature scaling (5). Since the plasma current is mainly driven by induction during L-mode discharges, the effect of the self-generated noninductive bootstrap current is neglected in this model. The plasma resistivity $\eta\left(T_e\right)$ is given by

$$\eta\left(\hat{\rho}, t\right) = \frac{k_{\text{eff}} Z_{\text{eff}}}{T_e^{3/2}\left(\hat{\rho}, t\right)} \tag{7}$$

where k_{eff} is a constant. The effective atomic number of the plasma, Z_{eff}, is considered to be constant in this model.

The models (5)–(7) allow us to write the magnetic diffusion (3) as

$$\frac{\partial \psi}{\partial t} = f_1\left(\hat{\rho}\right) u_1(t) \frac{1}{\hat{\rho}} \frac{\partial}{\partial \hat{\rho}} \left(\hat{\rho} f_4\left(\hat{\rho}\right) \frac{\partial \psi}{\partial \hat{\rho}}\right) + f_2\left(\hat{\rho}\right) u_2(t) \tag{8}$$

with boundary conditions given by

$$\left.\frac{\partial \psi}{\partial \hat{\rho}}\right|_{\hat{\rho}=0} = 0, \quad \left.\frac{\partial \psi}{\partial \hat{\rho}}\right|_{\hat{\rho}=1} = -k_3 u_3(t) \tag{9}$$

where

$$f_1\left(\hat{\rho}\right) = \frac{k_{\text{eff}} Z_{\text{eff}}}{k_{T_e}^{3/2} \mu_0 \rho_b^2 \hat{F}^2\left(\hat{\rho}\right)\left(T_e^{\text{profile}}\left(\hat{\rho}\right)\right)^{3/2}} \tag{10}$$

$$f_2\left(\hat{\rho}\right) = \frac{k_{\text{eff}} Z_{\text{eff}} R_0 k_{\text{NI}} \hat{H}\left(\hat{\rho}\right) j_{\text{NI}}^{\text{profile}}\left(\hat{\rho}\right)}{k_{T_e}^{3/2}\left(T_e^{\text{profile}}\left(\hat{\rho}\right)\right)^{3/2}} \tag{11}$$

$$f_4\left(\hat{\rho}\right) = \hat{F}\left(\hat{\rho}\right)\hat{G}\left(\hat{\rho}\right)\hat{H}\left(\hat{\rho}\right), \; k_3 = \frac{\mu_0}{2\pi}\frac{R_0}{\hat{G}\big|_{\hat{\rho}=1}\hat{H}\big|_{\hat{\rho}=1}} \tag{12}$$

$$u_1(t) = \left(\frac{\bar{n}(t)}{I(t)\sqrt{P_{\text{tot}}(t)}}\right)^{3/2}, \; u_2(t) = \frac{\sqrt{P_{\text{tot}}(t)}}{I(t)}, \; u_3(t) = I(t). \tag{13}$$

Equation (8) admits diffusivity, interior, and boundary actuators u_1, u_2, and u_3, respectively, which each represent nonlinear combinations of the physical actuators, $I(t)$, $P_{\text{tot}}(t)$, and $\bar{n}(t)$. Note that the controller proposed in this paper will generate waveforms for these physical actuators. These waveforms represent references to be sent to existing dedicated controllers for each of the respective quantities.

We expand (8) with the chain rule to obtain

$$\frac{\partial \psi}{\partial t} = f_1 u_1(t) \frac{1}{\hat{\rho}} \left(\hat{\rho} \frac{\partial \psi}{\partial \hat{\rho}} \frac{\partial f_4}{\partial \hat{\rho}} + f_4 \frac{\partial \psi}{\partial \hat{\rho}} + \hat{\rho} f_4 \frac{\partial^2 \psi}{\partial \hat{\rho}^2}\right) + f_2 u_2(t). \tag{14}$$

We then insert (2) into (14), resulting in

$$\frac{\partial \psi}{\partial t} = f_1 u_1 \frac{1}{\hat{\rho}} \left(\hat{\rho}\theta f_4' + f_4\theta + \hat{\rho} f_4 \theta'\right) + f_2 u_2 \tag{15}$$

where $(\cdot)' = \partial/\partial\hat{\rho}$ and the dependencies on time and space have been dropped to simplify the representation. By differentiating (15) with respect to $\hat{\rho}$, the PDE governing the evolution of $\theta\left(\hat{\rho}, t\right)$ is found to be

$$\frac{\partial \theta}{\partial t} = h_0 u_1 \theta'' + h_1 u_1 \theta' + h_2 u_1 \theta + h_3 u_2 \tag{16}$$

with boundary conditions

$$\theta\big|_{\hat{\rho}=0} = 0, \qquad \theta\big|_{\hat{\rho}=1} = -k_3 u_3 \tag{17}$$

and where h_0, h_1, h_2, and h_3 are spatially varying functions given by

$$h_0 = f_1 f_4 \tag{18}$$

$$h_1 = f_1' f_4 + f_1 f_4 \frac{1}{\hat{\rho}} + 2 f_1 f_4' \tag{19}$$

$$h_2 = f_1' f_4' + f_1' f_4 \frac{1}{\hat{\rho}} + f_1 f_4' \frac{1}{\hat{\rho}} - f_1 f_4 \frac{1}{\hat{\rho}^2} + f_1 f_4'' \tag{20}$$

$$h_3 = f_2'. \tag{21}$$

III. Control Objective

Let $u_{ff}(t) = [u_{1_{ff}}(t), \; u_{2_{ff}}(t), \; u_{3_{ff}}(t)]$ represent a set of feedforward control input trajectories and $\theta_{ff}(\hat{\rho}, t)$ be the associated poloidal flux gradient profile evolution for a nominal initial condition $\theta_{ff}(\hat{\rho}, 0)$. We note that the feedforward input and profile trajectories could be chosen based on the results of experimental testing or from offline optimization

using the current profile evolution model, as was done in [20] and [21]. The nominal profile evolution satisfies

$$\frac{\partial \theta_{ff}}{\partial t} = u_{1_{ff}}\left(h_0\theta''_{ff} + h_1\theta'_{ff} + h_2\theta_{ff}\right) + h_3 u_{2_{ff}} \quad (22)$$

$$\theta_{ff}\big|_{\hat{\rho}=0} = 0, \qquad \theta_{ff}\big|_{\hat{\rho}=1} = -k_3 u_{3_{ff}}. \quad (23)$$

Given errors in the initial conditions or other disturbances, the actual state will differ from the desired target, i.e., $\theta(\hat{\rho}, t) = \theta_{ff}(\hat{\rho}, t) + \tilde{\theta}(\hat{\rho}, t)$, where $\tilde{\theta}$ represents the error between the achieved and desired profile. Since the feedforward inputs are calculated offline, they cannot compensate for these deviations, so we consider the addition of feedback control to actively regulate the poloidal flux gradient profile around the desired profile evolution. Because of the strong influence of the boundary actuator on the dynamics of the system, we will consider the design of a feedback law for the boundary-control term u_3, i.e., we write $u_3 = u_{3_{ff}} + u_{3_{fb}}$. The incorporation of interior feedback control, which may enable improvements in closed-loop response, will be considered in future designs. The PDE (16) can then be written as

$$\frac{\partial\left(\theta_{ff} + \tilde{\theta}\right)}{\partial t} = u_{1_{ff}}\left[h_0\left(\theta''_{ff} + \tilde{\theta}''\right) + h_1\left(\theta'_{ff} + \tilde{\theta}'\right) + h_2\left(\theta_{ff} + \tilde{\theta}\right)\right] + h_3 u_{2_{ff}} \quad (24)$$

with the boundary conditions (17) becoming

$$\left(\theta_{ff} + \tilde{\theta}\right)\big|_{\hat{\rho}=0} = 0, \quad \left(\theta_{ff} + \tilde{\theta}\right)\big|_{\hat{\rho}=1} = -k_3\left(u_{3_{ff}} + u_{3_{fb}}\right). \quad (25)$$

Noting (22) and (23), these expressions can be reduced to

$$\frac{\partial \tilde{\theta}}{\partial t} = h_0 u_{1_{ff}}\tilde{\theta}'' + h_1 u_{1_{ff}}\tilde{\theta}' + h_2 u_{1_{ff}}\tilde{\theta} \quad (26)$$

with boundary conditions

$$\tilde{\theta}\big|_{\hat{\rho}=0} = 0, \qquad \tilde{\theta}\big|_{\hat{\rho}=1} = -k_3 u_{3_{fb}}. \quad (27)$$

The control design objective is then to force $\tilde{\theta}$ to zero by augmenting the feedforward control trajectories with a boundary feedback term $u_{3_{fb}}$.

IV. Backstepping Boundary Controller

A backstepping technique is used to transform a spatially discretized form of the original system of equations into an asymptotically stable target system. Then, by applying the inverse of the transformation to the boundary condition of the target system, a stabilizing boundary feedback law for the discretized model is found. The technique is shown in Fig. 4.

A. Controller Design

By defining $h = 1/N$, where N is an integer, and using the notation $x^i(t) = x(ih, t)$, the model (26) can be written as

$$\dot{\tilde{\theta}}^i = h_0^i u_{1_{ff}}\frac{\tilde{\theta}^{i+1} - 2\tilde{\theta}^i + \tilde{\theta}^{i-1}}{h^2} + h_1^i u_{1_{ff}}\frac{\tilde{\theta}^{i+1} - \tilde{\theta}^{i-1}}{2h} + h_2^i u_{1_{ff}}\tilde{\theta}^i \quad (28)$$

with boundary conditions (27) written

$$\tilde{\theta}^0 = 0, \qquad \tilde{\theta}^N = -k_3 u_{3_{fb}}. \quad (29)$$

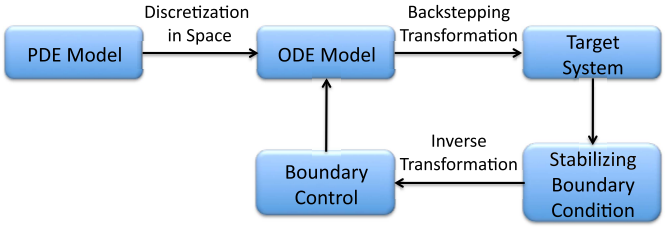

Fig. 4. Backstepping control technique.

We choose the following asymptotically stable target system:

$$\frac{\partial \tilde{w}}{\partial t} = h_0 u_{1_{ff}}\tilde{w}'' + h_1 u_{1_{ff}}\tilde{w}' + h_2 u_{1_{ff}}\tilde{w} - C_w(\hat{\rho})u_{1_{ff}}\tilde{w} \quad (30)$$

with boundary conditions

$$\tilde{w}\big|_{\hat{\rho}=0} = 0, \qquad \tilde{w}\big|_{\hat{\rho}=1} = 0. \quad (31)$$

The choice of target system is motivated by the need to maintain the parabolic character of the PDE (26) (to keep the highest order derivatives) while improving upon the performance of the system. The design parameter $C_w(\hat{\rho}) > 0$ is chosen based on a tradeoff between desired levels of robustness and performance and the physical actuator limits and can be chosen to weight parts of the profile more than others. The target system (30) can be spatially discretized as

$$\dot{\tilde{w}}^i = h_0^i u_{1_{ff}}\frac{\tilde{w}^{i+1} - 2\tilde{w}^i + \tilde{w}^{i-1}}{h^2} + h_1^i u_{1_{ff}}\frac{\tilde{w}^{i+1} - \tilde{w}^{i-1}}{2h} + h_2^i u_{1_{ff}}\tilde{w}^i - C_w^i u_{1_{ff}}\tilde{w}^i \quad (32)$$

with boundary conditions (31) written as

$$\tilde{w}^0 = 0, \qquad \tilde{w}^N = 0. \quad (33)$$

Next, a backstepping transformation is sought in the form

$$\tilde{w}^i = \tilde{\theta}^i - \alpha^{i-1}\left(\tilde{\theta}^0, \ldots, \tilde{\theta}^{i-1}\right). \quad (34)$$

By subtracting (32) from (28), the expression $\dot{\alpha}^{i-1} = \dot{\tilde{\theta}}^i - \dot{\tilde{w}}^i$ is obtained in terms of $\alpha^{k-1} = \tilde{\theta}^k - \tilde{w}^k$, $k = i-1, i, i+1$

$$\dot{\alpha}^{i-1} = h_0^i u_{1_{ff}}\frac{\alpha^i - 2\alpha^{i-1} + \alpha^{i-2}}{h^2} + h_1^i u_{1_{ff}}\frac{\alpha^i - \alpha^{i-2}}{2h} + h_2^i u_{1_{ff}}\alpha^{i-1} + C_w^i u_{1_{ff}}\tilde{\theta}^i - C_w^i u_{1_{ff}}\alpha^{i-1} \quad (35)$$

which can be solved for α^i to yield

$$\alpha^i = -\left[\frac{1}{\frac{h_0^i}{h^2} + \frac{h_1^i}{2h}}\right]\left[\left(\frac{-2h_0^i}{h^2} + h_2^i - C_w^i\right)\alpha^{i-1} + \left(\frac{h_0^i}{h^2} - \frac{h_1^i}{2h}\right)\alpha^{i-2} - \frac{1}{u_{1_{ff}}}\dot{\alpha}^{i-1} + C_w^i\tilde{\theta}^i\right] \quad (36)$$

where $\alpha^0 = 0$ and $\dot{\alpha}^{i-1}$ is calculated as

$$\dot{\alpha}^{i-1} = \sum_{k=1}^{i-1}\frac{\partial \alpha^{i-1}}{\partial \tilde{\theta}^k}\dot{\tilde{\theta}}^k. \quad (37)$$

Next, subtracting (33) from (29) and putting the resulting expression in terms of $\alpha^{k-1} = \tilde{\theta}^k - \tilde{w}^k,\ k = i-1, i, i+1$, the control law for $u_{3_{fb}}$ can be defined as

$$u_{3_{fb}} = -\frac{1}{k_3}\alpha^{N-1}. \tag{38}$$

For any choice of grid size N, the control law (38) will be a time-invariant linear combination of $N-1$ measurements from the interior of the plasma. The coefficients of this linear combination can be calculated ahead of time for a given set of model parameters h_0, h_1, and h_2, and are independent of the feedforward inputs and trajectories. To aid in the recursive calculation of the coefficients, we define $\Phi \in \mathbb{R}^{N-1\times N}$ for which the elements of column $i+1$ represent the coefficients of the $\tilde{\theta}$ measurements used to evaluate α^i

$$\alpha^i = \sum_{j=1}^{i} \Phi_{j,i+1}\tilde{\theta}^j \tag{39}$$

for $1 \le i \le N-1$. The first column (associated with $i=0$) is all zeros since $\alpha^0 = 0$. We note that we can then write

$$\dot{\alpha}^i = \sum_{j=1}^{i} \Phi_{j,i+1}\dot{\tilde{\theta}}^j. \tag{40}$$

We substitute (28) into this expression, yielding

$$\frac{\dot{\alpha}^i}{u_{1_{ff}}} = \sum_{j=1}^{i} \Phi_{j,i+1}\left[h_0^j\frac{\tilde{\theta}^{j+1} - 2\tilde{\theta}^j + \tilde{\theta}^{j-1}}{h^2} + h_1^j\frac{\tilde{\theta}^{j+1} - \tilde{\theta}^{j-1}}{2h} + h_2^j\tilde{\theta}^j\right]$$

for $1 \le i \le N-2$ (we do not need to evaluate at $N-1$ to calculate the control law). This term is also a time invariant linear combination of measurements, so we define a matrix $\Psi \in \mathbb{R}^{N-1\times N}$ for which the elements of column $i+1$ represent the measurement coefficients needed to evaluate $\dot{\alpha}^i/u_{1_{ff}}$

$$\frac{\dot{\alpha}^i}{u_{1_{ff}}} = \sum_{j=1}^{i+1} \Psi_{j,i+1}\tilde{\theta}^j. \tag{41}$$

The first column of Ψ is all zeros since $\dot{\alpha}^0 = 0$. We can then write (36) as

$$\begin{aligned}\alpha^i &= \sum_{j=1}^{i} \Phi_{j,i}\tilde{\theta}^j \\ &= -\left[\frac{1}{\frac{h_0^i}{h^2} + \frac{h_1^i}{2h}}\right] \\ &\quad\times\left[\left(\frac{-2h_0^i}{h^2} + h_2^i - C_w^i\right)\sum_{j=1}^{i-1}\Phi_{j,i-1}\tilde{\theta}^j + \left(\frac{h_0^i}{h^2} - \frac{h_1^i}{2h}\right)\right. \\ &\qquad\left.\times\sum_{j=1}^{i-2}\Phi_{j,i-2}\tilde{\theta}^j - \sum_{j=1}^{i}\Psi_{j,i}\tilde{\theta}^j + C_w^i\tilde{\theta}^i\right].\end{aligned} \tag{42}$$

Starting with $\alpha^0 = 0$ and $\dot{\alpha}^0 = 0$, expressions (41) and (42) for $i = 1, \ldots, N$ can be used to recursively fill the columns of Φ and Ψ. The control law (38) can then be written in the explicit feedback form

$$u_{3_{fb}} = -\tfrac{1}{k_3}\sum_{j=1}^{N-1}\Phi_{j,N}\tilde{\theta}^j. \tag{43}$$

The control law (43) allows us to calculate $u_{3_{fb}}$, which is then added to $u_{3_{ff}}$. The new value of u_3 is subsequently used with the feedforward trajectories u_2 and u_1 in the nonlinear transformations

$$I_p = u_3 \tag{44}$$

$$P_{\text{tot}} = u_3^2 u_{2_{ff}}^2 \tag{45}$$

$$\bar{n} = u_{1_{ff}}^{2/3} u_3^2 u_{2_{ff}} \tag{46}$$

to calculate the input requests I_p, P_{tot}, and $\bar{n}$. In experimental testing, these requests are then sent as references to the respective dedicated controllers on the DIII-D device.

B. Stability of the Target System

To facilitate the proof of stability of the chosen target system, we first write the discretized target system (32) and (33) as a matrix equation. By noting the boundary conditions (31), and defining $\mathbf{C}_w$ as a square diagonal matrix populated with the values of C_w^i for $1 \le i \le N-1$, the set of ODEs describing the target system can be expressed as

$$\dot{\beta}(t) = (M - \mathbf{C}_w)\,\beta(t)u_{1_{ff}}(t) \tag{47}$$

where $\beta = \left[\tilde{w}^1, \ldots, \tilde{w}^{N-1}\right]^T \in \mathbb{R}^{N-2\times 1}$ is the value of $\tilde{w}^i$ at the interior nodes, and the elements of the system matrix $M \in \mathbb{R}^{N-1\times N-1}$ are defined as

$$M_{1,1} = h_2^1 - \frac{2h_0^1}{h^2}, \quad M_{N-1,N-1} = h_2^{N-1} - \frac{2h_0^{N-1}}{h^2} \tag{48}$$

$$M_{1,2} = \frac{h_0^1}{h^2} + \frac{h_1^1}{2h}, \quad M_{N-1,N-2} = \frac{h_0^{N-1}}{h^2} - \frac{h_1^{N-1}}{2h} \tag{49}$$

$$M_{i,i-1} = \frac{h_0^i}{h^2} - \frac{h_1^i}{2h}, \quad M_{i,i} = h_2^i - \frac{2h_0^i}{h^2} \tag{50}$$

$$M_{i,i-1} = \frac{h_0^i}{h^2} + \frac{h_1^i}{2h}, \quad \text{for} \quad 2 \le i \le (N-2). \tag{51}$$

The remaining entries in the M matrix are all zero. Taking $V = 1/2\beta^T\Gamma\beta$ as a Lyapunov functional, where Γ is a positive definite matrix. We can compute the time derivative as

$$\dot{V} = \beta^T\Gamma\dot{\beta} = \beta^T\Gamma\,(M - \mathbf{C}_w)\,u_{1_{ff}}(t)\beta. \tag{52}$$

Since $u_{1_{ff}}(t) > 0\ \forall t$ and Γ is positive definite, we have that $(M - \mathbf{C}_w)$ must be negative definite to ensure that $\dot{V}$ is negative definite for $\beta \neq 0$. For the model parameters used in this paper, which are representative of a particular DIII-D discharge, M is negative definite and, since $\mathbf{C}_w \ge 0$, we can be sure that the matrix $(M - \mathbf{C}_w)$ is negative definite. As a result, the discretized target system is asymptotically stable. It can be seen from this analysis how the choice of $\mathbf{C}_w$ can adjust the speed of response of the system. A detailed study of the stability properties of the open-loop current profile dynamics can be found in [43].

C. Adaptive Law for Disturbance Rejection

The feedback law (43) is designed to improve upon the speed of response and stability properties of the current profile in the event of perturbed initial conditions. To improve upon the disturbance rejection capabilities of the controller, we augment the backstepping control law with an adaptive law that estimates a potential input disturbance on u_3 and effectively adds integral action to the closed-loop system. We consider the model (28) with the addition of a disturbance u_{3_d} at the boundary, such that the boundary conditions (29) become

$$\tilde{\theta}^0 = 0, \qquad \tilde{\theta}^N = -k_3\left(u_{3_{fb}} + u_{3_d}\right). \tag{53}$$

We follow the same backstepping procedure as before to obtain the recursively calculated transformation (36). If the disturbance were a known quantity, we could find the control law for $u_{3_{fb}}$ by subtracting (33) from (53) and putting the result in terms of $\alpha^{k-1} = \tilde{\theta}^k - \tilde{w}^k$, $k = i-1,\ i,\ i+1$. This would result in

$$u_{3_{fb}} = -\frac{1}{k_3}\alpha^{N-1} - u_{3_d} = -\frac{1}{k_3}\sum_{j=1}^{N-1}\Phi_{j,N}\tilde{\theta}^j - u_{3_d} \tag{54}$$

where the matrix Φ is found in the same way as shown in subsection IV-A. In practice, the disturbance is unknown and the controller must make use of an estimate $\hat{u}_{3_d}$, such that the control law becomes

$$u_{3_{fb}} = -\frac{1}{k_3}\sum_{j=1}^{N-1}\Phi_{j,N}\tilde{\theta}^j - \hat{u}_{3_d}. \tag{55}$$

If we apply the transformation (36) and the control law (55), the disturbed system is transformed to

$$\dot{\hat{w}}^i = u_{1_{ff}}\left(h_0^i\frac{\hat{w}^{i+1} - 2\hat{w}^i + \hat{w}^{i-1}}{h^2} + h_1^i\frac{\hat{w}^{i+1} - \hat{w}^{i-1}}{2h} + h_2^i\hat{w}^i - C_w^i\hat{w}^i\right) \tag{56}$$

with boundary conditions

$$\hat{w}^0 = 0 \tag{57}$$

$$\begin{aligned}\hat{w}^N &= \tilde{\theta}^N - \hat{\alpha}^{N-1}\\ &= -k_3\left(u_{3_{fb}} + u_{3_d}\right) + k_3\left(u_{3_{fb}} + \hat{u}_{3_d}\right)\\ &= k_3\tilde{u}_{3_d}\end{aligned} \tag{58}$$

where $\tilde{u}_{3_d} = \hat{u}_{3_d} - u_{3_d}$ is the error in the estimate of the input disturbance. We now look for an adaptive law for the estimate $\hat{u}_{3_d}$ that guarantees stability of the target system.

We can write the achieved target system as a matrix equation. By noting the boundary conditions (57) and (58), the set of ODEs describing the target system can then be expressed as

$$\dot{\beta}(t) = (M - \mathbf{C}_w)\,\beta(t)u_{1_{ff}}(t) + Zu_{1_{ff}}(t)\tilde{u}_{3_d} \tag{59}$$

where β, M, and $\mathbf{C}_w$ are defined as before. The vector Z is all zeros except

$$Z_{N-1} = k_3\left(\frac{h_0^{N-1}}{h^2} + \frac{h_1^{N-1}}{2h}\right). \tag{60}$$

We take

$$V = \frac{1}{2}\beta^T\Gamma\beta + \frac{C_3}{2}\tilde{u}_{3_d}^2 \tag{61}$$

as a Lyapunov functional, where Γ is a positive definite matrix and C_3 is a positive constant. We can then compute the time derivative as

$$\dot{V} = \beta^T\Gamma\dot{\beta} + C_3\tilde{u}_{3_d}\dot{\tilde{u}}_{3_d} \tag{62}$$

$$= \beta^T\Gamma\left(M - \mathbf{C}_w\right)u_{1_{ff}}(t)\beta + \beta^T\Gamma Z u_{1_{ff}}(t)\tilde{u}_{3_d} + C_3\tilde{u}_{3_d}\dot{\tilde{u}}_{3_d} \tag{63}$$

$$= \beta^T\Gamma\left(M - \mathbf{C}_w\right)u_{1_{ff}}(t)\beta + \left(\beta^T\Gamma Z u_{1_{ff}}(t) + C_3\dot{\tilde{u}}_{3_d}\right)\tilde{u}_{3_d}. \tag{64}$$

If we assume a constant disturbance and take the adaptive law

$$\dot{\tilde{u}}_{3_d} = \dot{\hat{u}}_{3_d} - \dot{u}_{3_d} = \dot{\hat{u}}_{3_d} = -\frac{u_{1_{ff}}(t)}{C_3}\beta^T\Gamma Z \tag{65}$$

we obtain

$$\dot{V} = \beta^T\Gamma\left(M - \mathbf{C}_w\right)u_{1_{ff}}(t)\beta. \tag{66}$$

As previously mentioned, M is negative definite for the model parameters used in this paper and, since, $\mathbf{C}_w \geq 0$, we can be sure that the matrix $(M - \mathbf{C}_w)$ is negative definite. Since $u_{1_{ff}}(t) > 0\ \forall t$, Γ is positive definite, and (61) is a function of β and $\tilde{u}_{3_d}$, $\dot{V}$ is negative semidefinite. Given that $\dot{u}_{ff}(t)$ is bounded, the conditions of Barbalat's lemma (see [44, p. 323]) are satisfied and we can be sure that $\dot{V} \to 0$ as $t \to \infty$, and, as a result, $\beta \to 0$. It can be seen from this analysis how the choice of $\mathbf{C}_w$ can adjust the speed of response of the system and C_3 determines the speed of adaptation.

We note that the matrix Φ can be used to write the vector of target system states, β, in terms of the vector of measurements $\Theta = [\tilde{\theta}^1, \ldots, \tilde{\theta}^{N-1}]^T$

$$\beta = \Theta - \Phi\Theta = (I - \Phi)\Theta. \tag{67}$$

This allows us to write the adaptive law as

$$\dot{\tilde{u}}_{3_d} = -\frac{u_{1_{ff}}(t)}{C_3}Z^T\Gamma^T\left(I - \Phi\right)\Theta. \tag{68}$$

The adaptive law (68) combined with the control law (43) allows for the calculation of the feedback term $u_{3_{fb}}$, which is then added to the feedforward term $u_{3_{ff}}$ to obtain u_3. The inputs u_1 and u_2 are again kept at their feedforward values. These signals are then used in the nonlinear transformations (44)–(46) to obtain the requests for I_p, P_{tot}, and $\bar{n}$.

V. Controller Implementation in the DIII-D PCS

In this section, we present the real-time control algorithm implementation in the DIII-D Plasma Control System (PCS) along with the simulation framework used to test the controller and ensure the real-time algorithm was working correctly prior to experiments.

A. Real-Time Algorithm

The real-time feedforward + feedback algorithm we have implemented in the DIII-D PCS is a general framework designed to enable testing of a variety of control laws, and can be used to control several different profiles and scalar quantities. Magnetic profiles that can be controlled include the safety factor, q, the rotational transform, $\iota = 1/q$, the poloidal magnetic flux, ψ, and the poloidal flux gradient, θ. Available kinetic profiles include the electron temperature, the ion temperature, and the toroidal rotation velocity. The framework can also be used to control scalar quantities, including normalized plasma beta β_N, the minimum q, or the internal inductance of the plasma, l_i. The rtEFIT code [45], a real-time magnetic equilibrium reconstruction code, and the real-time charge-exchange recombination (rtCER) code [46] were interfaced with the algorithm to provide measurements of magnetic and kinetic profiles on a grid of measurement points. Only the diagnostics from rtEFIT were needed for feedback in testing the controller presented in this paper. The real-time algorithm performs the necessary coordinate transformation to construct the variable of interest $\theta(\hat{\rho})$ from the data provided by rtEFIT [the plasma current $I(t)$, the poloidal stream function at the magnetic axis ψ_{axis} and the plasma boundary ψ_{bdry}, and the safety factor q at 64 evenly spaced points in the normalized flux spatial domain $\psi_n = (\psi - \psi_{\text{axis}})/(\psi_{\text{bdry}} - \psi_{\text{axis}})$]. The profile error $\tilde{\theta}$ is then generated by comparing the measurements to the target profile θ_{ff}. The feedback portion of the algorithm is a discrete time state-space system with a selectable sampling time. Based on the modulation rate of the motional Stark effect (MSE) beam used to obtain q profile measurements in real time, a sampling time of 20 ms was used in this paper (the beam was on for 10 ms and off for 10 ms). Taking the estimate of the input disturbance $\hat{u}_{3_d}$ as a controller state, the control laws (43) and (68) were put into a state-space form and a discrete time approximation with the appropriate sample time was generated. Within the PCS, the discrete state space control law produces the output u_{fb}, which is added to the feedforward signal, u_{ff}, before being passed to the nonlinear transformations (44)–(46). The resulting outputs $I(t)$, $P_{\text{tot}}(t)$, and $\bar{n}(t)$ are then sent as references to existing, empirically tuned single-input–single-output (SISO) control laws for the respective quantities. A proportional–integral–derivative (PID) loop is used to regulate the plasma current to the desired waveform via actuation of the ohmic coil voltage and measurements taken using a Rogowski loop. A separate PID controller is used to regulate the density through gas injection. The beam power is regulated through pulse width modulation of the power supplies for each neutral beam injector. While the current and beam controllers are typically effective and respond to reference changes at a time scale much faster than the current diffusion time scale, the density response can be slower, especially when being decreased. The experimental results presented in Section VII reflect this description (see Fig. 13). While this dynamic could be accounted for in future controller designs, it is not directly accounted for in the present design. Nevertheless, simulations and preliminary experimental results show that the closed-loop system is robust to poor density control to some degree. We have also included in the PCS framework the possibility of introducing artificial disturbances for testing through the signal u_d, and to specify target trajectories through the signal θ_{ff}. A block diagram representing the PCS implementation is given in Fig. 5.

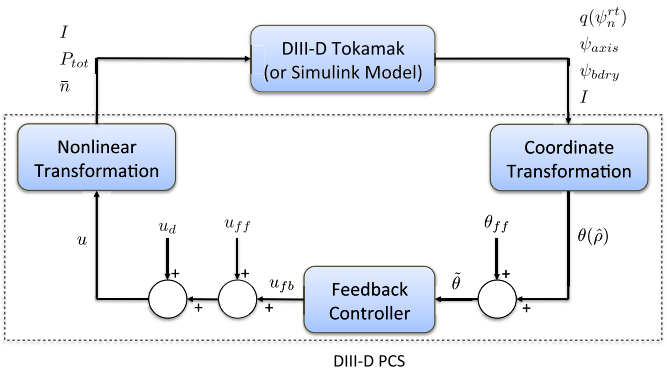

Fig. 5. DIII-D PCS implementation of the magnetic profile control algorithm. Note that the PCS code can either be connected to the DIII-D tokamak or, through the simserver architecture, a Simulink model of the magnetic diffusion equation for simulation tests.

B. Simserver Architecture

Prior to experimental testing, the control scheme proposed in this paper was evaluated through simulations using the simserver architecture, a simulation environment that allows the DIII-D PCS to exchange data with a MATLAB/Simulink model that generates simulated diagnostics. This framework enables debugging of the real-time feedback code as well as assessment of the effectiveness of control designs prior to actual experiments [47]. After the simulation phase, the same PCS code used in the simserver simulations was used to control the actual device. To test the control scheme proposed in this paper, a Simulink model of the magnetic diffusion (3) was integrated into a simserver and the real-time implementation of the control algorithm was programmed into the PCS [48]. The Simulink model was constructed by discretizing the magnetic diffusion equation in space and was made to output the same set of measurements sent to the PCS by rtEFIT during experiments.

VI. Simulation Results

In this section, we present results of the simulation study used to test and tune the controller design and implementation prior to experimental testing. The simulations presented here demonstrate the ability of the controller to track a desired profile evolution despite disturbances and perturbed initial conditions.

A. Simulation of Static Controller

For the results presented in this subsection, as well as for the experimental results, we used the static, nonadaptive control law (43) designed with $C_w^i = 3.75 \times 10^{-16}$ for $1 \leq i \leq 5$ and $C_w^i = 7.5 \times 10^{-16}$ for $6 \leq i \leq N$ where $N = 10$ (note that the simulation model was discretized on a finer grid than

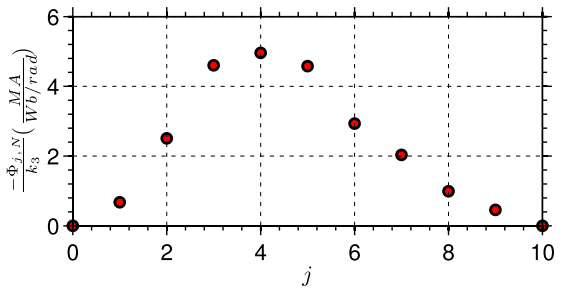

Fig. 6. Coefficients of the linear combination of profile errors that generate the feedback control term $u_{3_{fb}}$.

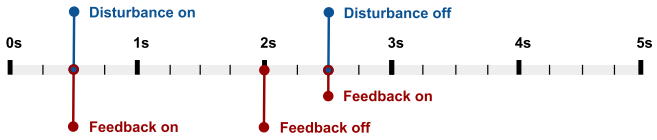

Fig. 7. Timeline depicting when the artificial disturbance and the feedback controller are switched on and off during the closed-loop simulation and the experimental shot 146454.

that used for control). The elements of the vector $-\Phi_{j,N}/k_3$, which represent the coefficients of the linear combination of profile errors that generate the feedback control term $u_{3_{fb}}$, are shown in Fig. 6. As designed, the largest weight is placed on profile errors around $j = 4$, corresponding to $\hat{\rho} = 0.4$.

In this simulation study, we tested the ability of the feedback controller to reject an artificially added input disturbance and to overcome errors in the initial condition of the profile. First, a particular set of feedforward inputs u_{ff} was used in a feedforward only simulation to generate a target poloidal flux gradient profile evolution θ_{ff}. The simulation was run again with the addition of an input disturbance of 0.1 MA (approximately 8%) to u_3 from $t = 0.5$ to 2.5 s. The feedback controller was activated from $t = 0.5$ to 2.0 s to test disturbance rejection and switched off from $t = 2.0$ to 2.5 s to observe how the profile would drift away from the desired one under the influence of the uncontrolled input disturbance. Finally, at $t = 2.5$ s, the controller was turned back on and the input disturbance was removed to see if the controller could recover the desired profile despite the profile error caused by the uncontrolled drift. The time intervals for which the system is disturbed and for which the feedback controller is turned on are summarized in Fig. 7.

Time traces of q at several points along the profile are shown in Fig. 8. The results of the closed-loop simulation are compared with the reference generated in the feedforward simulation without the disturbance. A small error remained during the disturbance rejection phase of the simulation (from $t = 0.5$ to 2.0 s). This can be expected since there is no integral action in the static controller. The steady-state error could be made smaller by increasing the gain of the controller (through the parameters C_w^i), however, this would increase the sensitivity of the closed-loop system to measurement noise. Subsequent simulation results will show that this problem can be avoided by using the adaptive law (68). When the controller was turned off from $t = 2.0$ to 2.5 s, the error caused by the boundary input disturbance [see Fig. 8(f)] diffused in from the edge of the plasma over time, reaching at least as far as $\hat{\rho} = 0.5$ before $t = 2.5$ s [see Fig. 8(c)]. At $t = 2.5$ s, the disturbance was removed and the controller was turned back on. The controller increased the value of q at the boundary [see Fig. 8(f)] and the effect of this increase diffused inward over time, causing the error initially present at $t = 2.5$ s to be removed.

B. Simulation of Adaptive Controller

Here, we present simulation results showing the improved disturbance rejection achieved with the addition of the adaptive law (68). The controller was designed, as in the previous case, using $C_w^i = 3.75 \times 10^{-16}$ for $1 \leq i \leq 5$ and $C_w^i = 7.5 \times 10^{-16}$ for $6 \leq i \leq N$ and with $N = 10$. For the adaptive law, we chose $C_3 = 1.5 \times 10^{-15}$ and $\Gamma = I$, where I is the identity matrix. The feedforward inputs used during this paper were the same as those used in the previous simulation and experiment. A disturbance in u_3 of -0.1 MA (approximately -8%) was applied from 0.5 s $\leq t <$ 2.5 s and a -0.2 MA disturbance (approximately -17%) was applied from 2.5 s $\leq t \leq$ 5.0 s. In addition, an unmatched disturbance of $+10\%$ in both u_1 and u_2 was applied throughout the discharge. A significant initial condition error was also imposed. Two simulation cases were run: 1) feedforward only and 2) feedforward + feedback using the adaptive law (68). The feedback controller was active throughout the second simulation. A timeline for the simulations is given in Fig. 9.

In Fig. 10, the q and θ profiles achieved in each of the simulation cases are compared with the target profiles at several times. The first three plots [Fig. 10(a)–(c)] show results during the first disturbance ($+10\%$ in u_1 and u_2, -0.1 MA in u_3), while [Fig. 10(d)–(f)] show results during the second disturbance ($+10\%$ in u_1 and u_2, -0.2 MA in u_3). The disturbances caused the open-loop profiles to differ significantly from the target profiles. On the other hand, the adaptive backstepping controller was able to quickly reject the disturbances and match the target profile after a short time, as visible in Fig. 10(c) and (f). Even with the presence of unmatched disturbances, the controller was able to achieve excellent regulation of the desired target profile. It is expected that adding feedback control laws for the interior and diffusive actuators u_1 and u_2 could improve upon the results by adding extra degrees of freedom to the control scheme.

VII. Experimental Testing

The goal of the experiment presented here was to verify that the feedback controller synthesized from a first-principles-based model of the poloidal flux profile evolution is able to drive the poloidal flux gradient profile in the DIII-D device to a desired target. While the feedback scheme could eventually be used to attempt to track an arbitrarily chosen target, we began by testing the controller using a target that is known to be achievable. We guaranteed the achievability of the target profile by generating it from the results of the open-loop shot 145477 using the same feedforward inputs as those used in

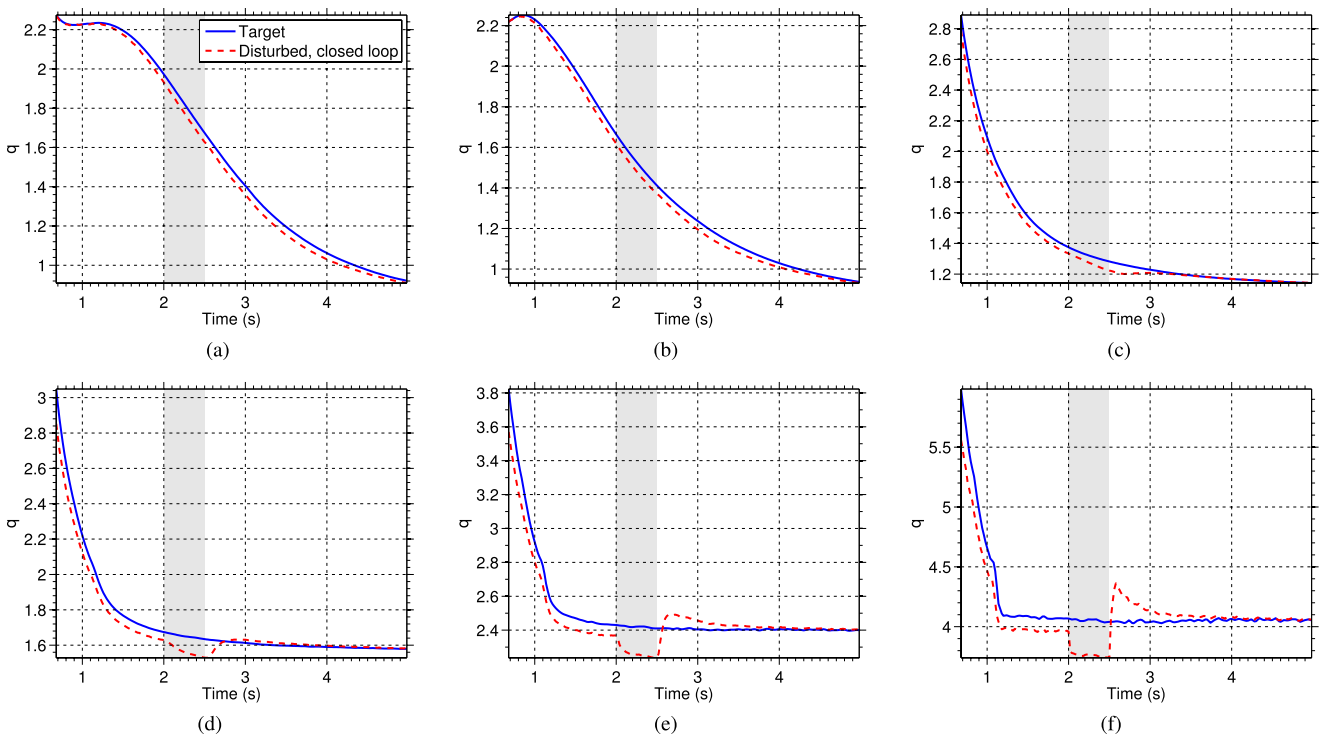

Fig. 8. Time traces of q at various points comparing the nominal feedforward simulation (blue-solid line) with the closed loop, disturbed simulation (red-dashed line) using the static control law. Note the effect of turning off the controller between $t = 2.0$ s and $t = 2.5$ s (shaded regions on the plots). (a) $\hat{\rho} = 0.1$. (b) $\hat{\rho} = 0.25$. (c) $\hat{\rho} = 0.5$. (d) $\hat{\rho} = 0.65$. (e) $\hat{\rho} = 0.8$. (f) $\hat{\rho} = 0.95$.

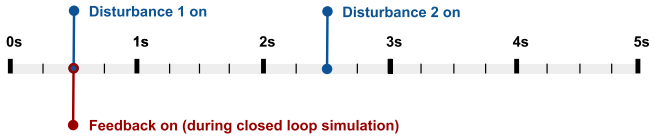

Fig. 9. Timeline depicting when the artificial disturbance and the adaptive feedback controller are switched on and off during the closed-loop simulation.

the simulation study. The reference scenario was a double-null plasma with a toroidal magnetic field of 1.85 T, and flat-top values of I_p, $\bar{n}$, and β_N (a normalized figure of merit for plasma performance) of 1.2 MA, 2×10^{19} m^{-3}, and 0.8%, respectively. The resulting θ profile was then used as the target for the closed loop (feedforward + feedback) shot 146 454. During shot 146 454, we used the static control law (43) designed with $C_w^i = 3.75 \times 10^{-16}$ for $1 \leq i \leq 5$ and $C_w^i = 7.5 \times 10^{-16}$ for $6 \leq i \leq N$ where $N = 10$. In addition, an input disturbance of 0.1 MA in the reference for u_3 was added from $t = 0.5$ to 2.5 s. The feedback controller was turned on from $t = 0.5$ to 2.0 s to test disturbance rejection and switched off from $t = 2.0$ to 2.5 s to allow the θ profile to drift away from the desired one under the influence of the input disturbance. Finally, at $t = 2.5$ s the controller was turned back on and the input disturbance was removed to see if the controller could recover the desired profile despite the error caused by the drift. This is the same scenario that was used in the first simulation results and shown in Fig. 7.

Time traces of q at several points along the profile are given in Fig. 11. The results of the closed-loop shot 146 454 are compared with the reference generated in the feedforward shot 145 477. During the closed-loop shot, there was an initial condition error, which can most clearly be seen in Fig. 11(b) and (c), in addition to the artificially applied input disturbance. Though the controller mostly rejected the disturbance during the first phase ($t = 0.5$ to 2.0 s), a small amount of error remained at the end of the controlled interval [see Fig. 11(f)]. As was mentioned before, this offset is because the backstepping controller is static, i.e., it contains only proportional feedback and no integral action. The offset could be reduced by increasing the gain of the controller, however, this would increase the sensitivity to noise and may cause the controller to be too aggressive. The addition of the adaptive law (68), which will be tested in a future experimental campaign, should improve upon the disturbance rejection and tracking capabilities of this scheme, as was demonstrated in simulations. The error caused by the disturbance increased when the controller was turned off, and the error diffused in from the edge of the plasma throughout the brief uncontrolled drift phase ($t = 2.0$ to 2.5 s), as can be seen in [Fig. 11(c)–(f)]. Finally, once the disturbance was removed and the controller was turned back on at $t = 2.5$ s, the target values of q were quickly recovered.

In Fig. 12, the q and θ profiles achieved in the closed loop, disturbed shot 146 454 are compared with the desired reference profiles obtained from shot 145 477 at several times. Fig. 12(a) shows that the controller partially rejected the disturbance and achieved a profile close to the desired one shortly before it was turned off at $t = 2.0$ s. Fig. 12(b) shows the error resulting from the disturbance after the

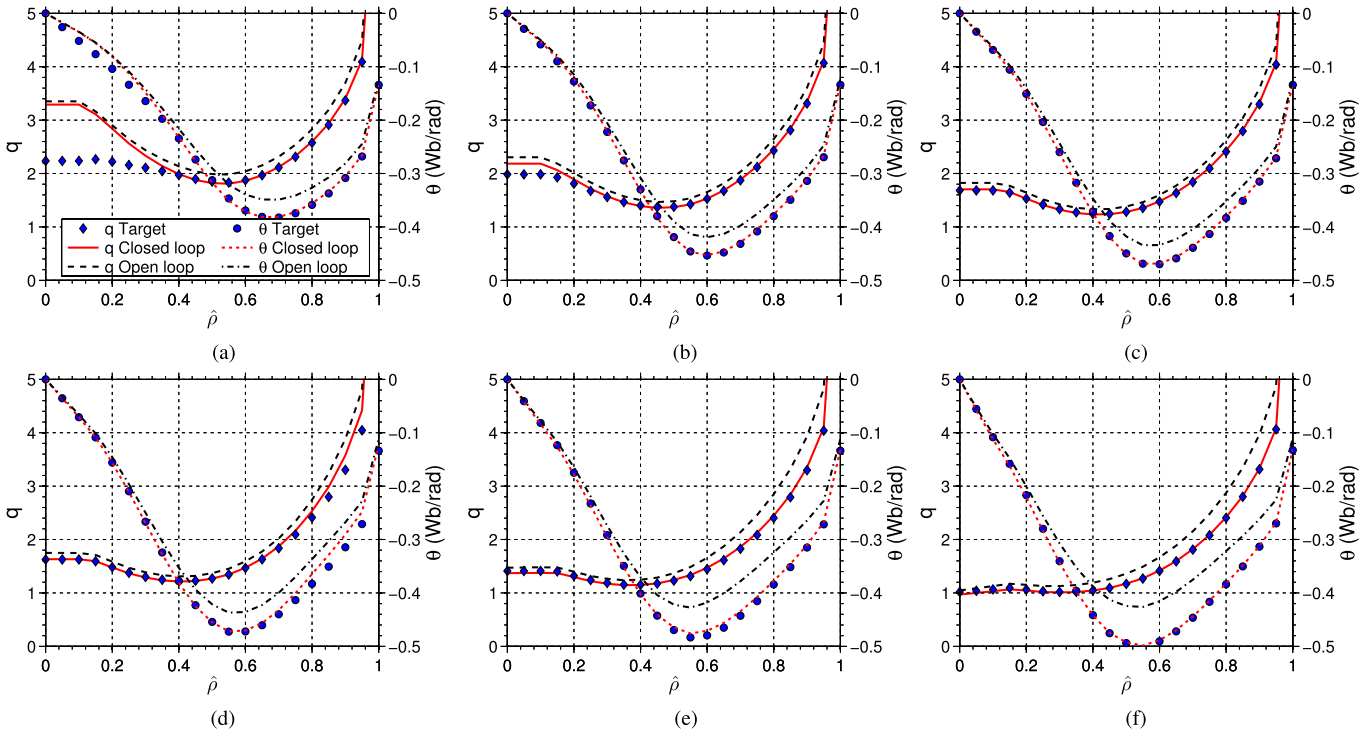

Fig. 10. Comparison of q and θ profiles at various times for the adaptive control simulation. The open loop, feedforward only profiles (q: black, dashed, θ: black, dash-dot) and closed-loop profiles (q: red, solid, θ: red, dotted) are compared with the desired target (q: blue diamond markers, θ: blue circular markers). (a) $t = 1.2$ s. (b) $t = 2.0$ s. (c) $t = 2.5$ s. (d) $t = 2.6$ s. (e) $t = 3.0$ s. (f) $t = 4.0$ s.

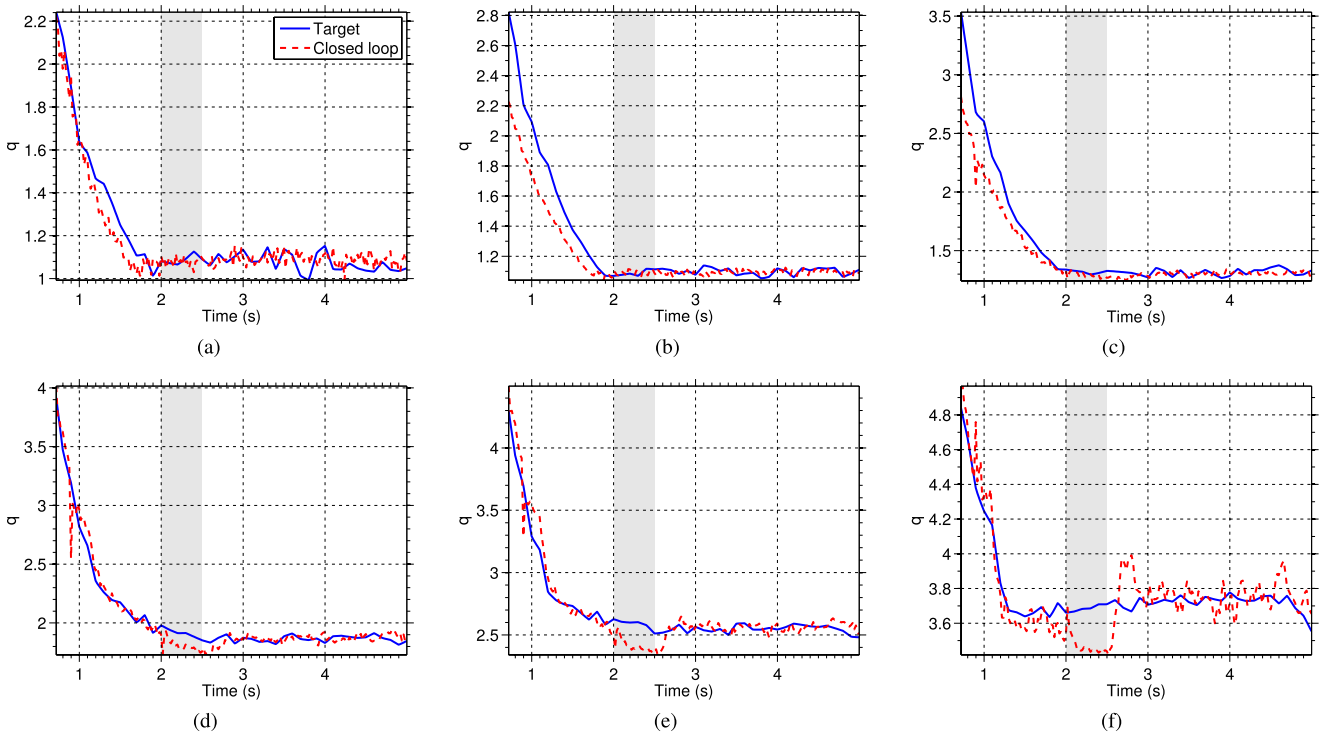

Fig. 11. Time traces of q at various points comparing the experimental results for the reference shot 145 477 (blue-solid line) and the closed loop, disturbed shot 146 454 (red-dashed line). Note the effect of turning off the controller during the interval 2.0 s $\leq t \leq$ 2.5 s (shaded regions of plots). (a) $\hat{\rho} = 0.1$. (b) $\hat{\rho} = 0.25$. (c) $\hat{\rho} = 0.5$. (d) $\hat{\rho} = 0.65$. (e) $\hat{\rho} = 0.8$. (f) $\hat{\rho} = 0.95$.

brief uncontrolled drift phase ($t = 2.0$ to 2.5 s), while the successful recovery of the desired profile after the controller was turned back on is clearly seen in Fig. 12(c). The red shaded regions, which represent the standard deviation of the measurements over a 0.25 s window prior to the time shown, provide an indication of the measurement noise.

Finally, the actuator requests and achieved values are compared in Fig. 13. It should be noted that while the total plasma

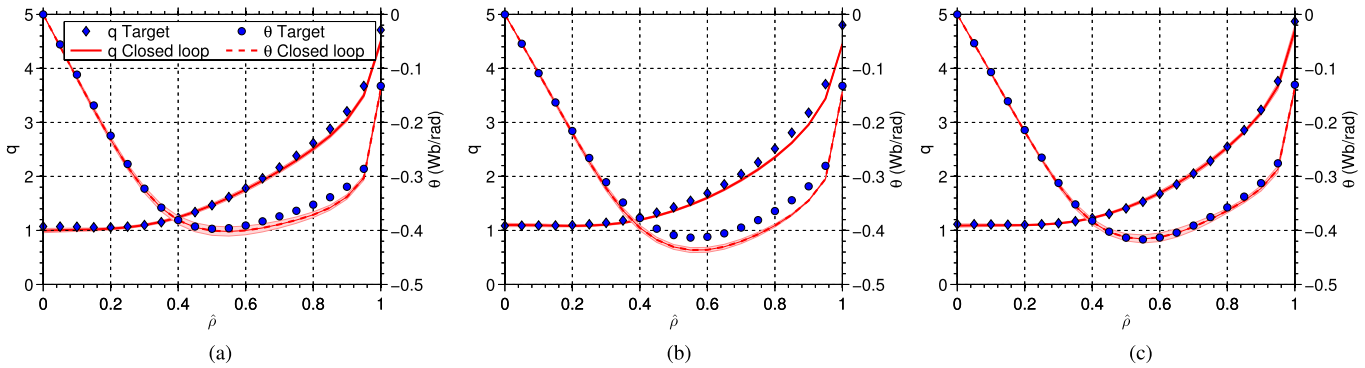

Fig. 12. Comparison of experimentally achieved q and θ profiles at various times for reference shot 145477 (q: blue diamond markers, θ, blue circular markers) and the closed loop, disturbed shot 146454 (q: red-solid, θ: red-dashed). (a) $t = 1.98$ s, feedback and disturbance on. (b) $t = 2.5$ s, feedback off, disturbance on. (c) $t = 4.02$ s, feedback on, disturbance off. The red shaded regions represent the standard deviation of the measurements over a 0.25 s window prior to the time shown.

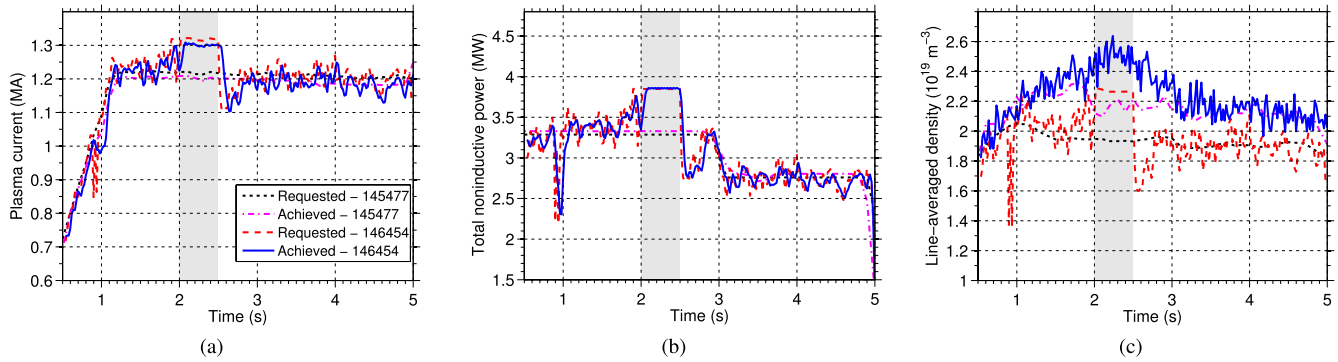

Fig. 13. Comparison of requested and achieved actuator values during the feedforward shot 145477 and the closed loop, disturbed shot 146454. During the closed-loop shot, the feedback control was turned off between $t = 2.0$ and 2.5 s (shaded regions of plots). (a) Plasma current I_p. (b) Total noninductive power P_{tot}. (c) Line averaged density $\bar{n}$.

current and total power were tightly controlled and the requests were reproduced quite well, the request for line averaged density was often not achieved. This represented additional input disturbances aside from the intentional one added to the feedforward input references.

VIII. Conclusion

We have presented a scheme for controlling the current profile in L-mode discharges in DIII-D based on a dynamic model of the evolution of the poloidal magnetic flux profile. By employing a backstepping control design technique, a transformation was found from the spatially discretized system to an asymptotically stable target system, along with a boundary feedback control law. The resulting control law is designed to augment an arbitrary set of feedforward input trajectories. We have also presented an adaptive law to add integral action to the control scheme. Through a nonlinear transformation of the control inputs, the scheme provides stabilizing reference values for the total plasma current, noninductive power, and plasma density. A simulation study shows the performance of the controller when initial conditions are perturbed and the input is biased. Preliminary experimental results are also presented, showing the controller to perform well despite the presence of additional disturbances caused by the physical actuators and noisy real-time measurements of the θ profile. Experimental testing of the adaptive scheme presented in this paper will be carried out in future campaigns.

While the controller was designed using a model that best describes the early, inductive phase of a plasma discharge, it performed well throughout the L-mode discharge it was tested on. This is likely because the self-generated noninductive current sources neglected in the model are typically small in L-mode discharges. Additional work will be needed to extend the model to H-mode scenarios, for which the self-generated noninductive current source becomes more significant. Work toward developing a nonlinear control-oriented PDE model of the poloidal magnetic flux profile during H-mode discharges will follow a similar approach to the one used in this paper. While boundary actuation will still have a strong influence on the profile evolution (especially during the ramp-up and early flattop phases of discharges), the increased fraction of noninductively driven current will motivate the design of additional interior actuator feedback laws in the control scheme. Additional degrees of freedom will be incorporated by separately modeling the effect of coinjection (on-axis/off-axis), counter injection, and balanced injection neutral beams, as well as electron cyclotron heating and current drive. In doing so, controllability of the current profile should be improved, expanding the set of achievable

profiles at steady-state. The long term goal of this paper is the development of first-principles-driven model-based feedforward + feedback control strategies for simultaneous control of the current profile and kinetic profiles (e.g., density and temperature) during H-mode discharges.

REFERENCES

[1] J. Wesson, *Tokamaks*, 3rd ed. Oxford, U.K.: Clarendon, 2004.

[2] J. P. Freidberg, *Ideal Magnetohydrodynamics*. New York, NY, USA: Plenum, 1987.

[3] A. Pironti and M. Walker, "Fusion, tokamaks, and plasma control: An introduction and tutorial," *IEEE Control Syst. Mag.*, vol. 25, no. 5, pp. 30–43, Oct. 2005.

[4] M. L. Walker, D. A. Humphreys, D. M. D. Mazon, M. Okabayashi, T. H. Osborne, and E. Schuster, "Emerging applications in tokamak plasma control. Control solutions for next-generation tokamaks," *IEEE Control Syst. Mag.*, vol. 26, no. 2, pp. 35–63, Apr. 2006.

[5] M. Murakami, M. R. Wade, C. M. Greenfield, T. C. Luce, J. R. Ferron, H. E. St John, *et al.*, "Progress toward fully noninductive, high beta conditions in DIII-D," *Phys. Plasmas*, vol. 13, no. 5, p. 056106, 2006.

[6] J. Ferron, P. Gohil, C. Greenfield, J. Lohr, T. C. Luce, M. A. Makowski, *et al.*, "Feedback control of the safety factor profile evolution during formation of an advanced tokamak discharge," *Nucl. Fusion*, vol. 46, pp. L13–L17, Oct. 2006.

[7] T. Wijnands, D. V. Houtte, G. Martin, X. Litaudon, and P. Froissard, "Feedback control of the current profile on Tore Supra," *Nucl. Fusion*, vol. 37, pp. 777–791, Jun. 1997.

[8] T. Suzuki, "Recent RF experiments and application of RF waves to real-time control of safety factor profile in JT-60U," in *Proc. AIP Conf.*, vol. 787. Apr. 2005, pp. 279–286.

[9] O. Barana, D. Mazon, L. Laborde, and F. Turco, "Feedback control of the lower hybrid power deposition profile on Tore Supra," *Plasma Phys. Controlled Fusion*, vol. 49, pp. 947–967, Jul. 2007.

[10] T. Suzuki, S. Ide, T. Oikawa, T. Fujita, M. Ishikawa, M. Seki, *et al.*, "Off-axis current drive and real-time control of current profile in JT-60U," *Nucl. Fusion*, vol. 48, p. 045002, Apr. 2008.

[11] D. Moreau, F. Crisanti, X. Litaudon, D. Mazon, P. De Vries, R. Felton, *et al.*, "Real-time control of the q-profile in JET for steady state advanced tokamak operation," *Nucl. Fusion*, vol. 43, pp. 870–882, Sep. 2003.

[12] L. Laborde, D. Mazon, D. Moreau, A. Murari, R. Felton, L. Zabeo, *et al.*, "A model-based technique for integrated real-time profile control in the JET tokamak," *Plasma Phys. Controlled Fusion*, vol. 47, pp. 155–183, Jan. 2005.

[13] D. Moreau, D. Mazon, M. Ariola, G. De Tommasi, L. Laborde, F. Piccolo, *et al.*, "A two-time-scale dynamic-model approach for magnetic and kinetic profile control in advanced tokamak scenarios on JET," *Nucl. Fusion*, vol. 48, p. 106001, Oct. 2008.

[14] W. Shi, W. Wehner, J. Barton, M. D. Boyer, E. Schuster, D. Moreau, *et al.*, "Multivariable robust control of the plasma rotational transform profile for advanced tokamak scenarios in DIII-D," in *Proc. Amer. Control Conf.*, 2012, pp. 5037–5042.

[15] W. Wehner, W. Shi, E. Schuster, D. Moreau, M. L. Walker, J. R. Ferron, *et al.*, "Optimal feedback control of the poloidal magnetic flux profile in the DIII-D tokamak based on identified plasma response models," in *Proc. Amer. Control Conf.*, 2012, pp. 5049–5054.

[16] D. Moreau, M. L. Walker, J. R. Ferron, F. Liu, E. Schuster, J. E. Barton, *et al.*, "Integrated magnetic and kinetic control of advanced tokamak plasmas on DIII-D based on data-driven models," *Nucl. Fusion*, vol. 53, no. 6, p. 063020, 2013.

[17] Y. Ou, T. Luce, E. Schuster, J. R. Ferron, M. L. Walker, C. Xu, *et al.*, "Towards model-based current profile control at DIII-D," *Fusion Eng. Des.*, vol. 82, pp. 1153–1160, Oct. 2007.

[18] E. Witrant, E. Joffrin, S. Bremond, G. Giruzzi, D. Mazon, O. Barana, *et al.*, "A control-oriented model of the current profile in tokamak plasma," *Plasma Phys. Controlled Fusion*, vol. 49, pp. 1075–1105, Jul. 2007.

[19] F. Felici, O. Sauter, S. Coda, B. Duval, T. Goodman, J.-M. Moret, *et al.*, "Real-time physics-model-based simulation of the current density profile in tokamak plasmas," *Nucl. Fusion*, vol. 51, no. 8, p. 083052, 2011.

[20] Y. Ou, C. Xu, E. Schuster, J. R. Ferron, M. L. Walker, and D. A. Humphreys, "Design and simulation of extremum-seeking open-loop optimal control of current profile in the DIII-D tokamak," *Plasma Phys. Controlled Fusion*, vol. 50, p. 115001, Nov. 2008.

[21] C. Xu, Y. Ou, J. Dalessio, E. Schuster, T. C. Luce, J. R. Ferron, *et al.*, "Ramp-up-phase current-profile control of tokamak plasmas via nonlinear programming," *IEEE Trans. Plasma Sci.*, vol. 38, no. 2, pp. 163–173, Feb. 2010.

[22] Y. Ou, C. Xu, and E. Schuster, "Robust control design for the poloidal magnetic flux profile evolution in the presence of model uncertainties," *IEEE Trans. Plasma Sci.*, vol. 38, no. 3, pp. 375–382, Mar. 2010.

[23] F. Argomedo, E. Witrant, C. Prieur, D. Georges, and S. Bremond, "Model-based control of the magnetic flux profile in a tokamak plasma," in *Proc. 49th IEEE CDC*, Dec. 2010, pp. 6926–6931.

[24] C. Xu, Y. Ou, and E. Schuster, "Sequential linear quadratic control of bilinear parabolic PDEs based on POD model reduction," *Automatica*, vol. 47, no. 2, pp. 418–426, 2011.

[25] Y. Ou, C. Xu, E. Schuster, T. C. Luce, J. R. Ferron, M. L. Walker, *et al.*, "Optimal tracking control of current profile in tokamaks," *IEEE Trans. Control Syst. Technol.*, vol. 19, no. 2, pp. 432–441, Mar. 2011.

[26] Y. Ou, C. Xu, E. Schuster, J. Ferron, T. Luce, M. Walker, *et al.*, "Receding-horizon optimal control of the current profile evolution during the ramp-up phase of a tokamak discharge," *Control Eng. Pract.*, vol. 19, no. 1, pp. 22–31, 2011.

[27] O. Gaye, E. Moulay, S. Bremond, L. Autrique, R. Nouailletas, and Y. Orlov, "Sliding mode stabilization of the current profile in tokamak plasmas," in *Proc. 50th IEEE CDC-ECC*, Dec. 2011, pp. 2638–2643.

[28] S. H. Kim and J. B. Lister, "A potentially robust plasma profile control approach for ITER using realtime estimation of linearized profile response models," *Nucl. Fusion*, vol. 52, no. 7, p. 074002, 2012.

[29] M. D. Boyer and E. Schuster, "Burn control in fusion reactors using simultaneous boundary and distributed actuation," in *Proc. 52nd IEEE CDC*, Dec. 2013, pp. 4188–4193.

[30] D. Boskovic, A. Balogh, and M. Krstic, "Backstepping in infinite dimension for a class of parabolic distributed parameter systems," *Math. Control, Signals, Syst.*, vol. 16, no. 1, pp. 44–75, 2003.

[31] M. Krstic and A. Smyshlyaev, *Boundary Control of PDEs*. Philadelphia, PA, USA: SIAM, 2008.

[32] D. Boskovic and M. Krstic, "Backstepping control of chemical tubular reactors," *Comput. Chem. Eng.*, vol. 26, pp. 1077–1085, Aug. 2002.

[33] D. Boskovic and M. Krstic, "Stabilization of a solid propellant rocket instability by state feedback," *Int. J. Robust Nonlinear Control*, vol. 13, pp. 483–495, Apr. 2003.

[34] E. Schuster and M. Krstić, "Control of a non-linear PDE system arising from non-burning tokamak plasma transport dynamics," *Int. J. Control*, vol. 76, pp. 1116–1124, Jan. 2003.

[35] D. Boyer and E. Schuster, "Simultaneous control of effective atomic number and electron density in non-burning tokamak plasmas," in *Proc. ACC*, Jun./Jul. 2010, pp. 1985–1990.

[36] M. D. Boyer and E. Schuster, "Backstepping control of density and energy profiles in a burning tokamak plasma," in *Proc. 50th IEEE CDC-ECC*, Dec. 2011, pp. 1993–1998.

[37] J. Barton, M. Boyer, W. Shi, E. Schuster, T. Luce, J. Ferron, *et al.*, "Toroidal current profile control during low confinement mode plasma discharges in DIII-D via first-principles-driven model-based robust control synthesis," *Nucl. Fusion*, vol. 52, no. 12, p. 123018, 2012.

[38] M. D. Boyer, J. Barton, E. Schuster, T. C. Luce, J. R. Ferron, M. L. Walker, *et al.*, "First-principles-driven model-based current profile control for the DIII-D tokamak via LQI optimal control," *Plasma Phys. Controlled Fusion*, vol. 55, p. 105007, Oct. 2013.

[39] F. L. Hinton and R. D. Hazeltine, "Theory of plasma transport in toroidal confinement systems," *Rev. Modern Phys.*, vol. 48, no. 2, pp. 239–308, 1976.

[40] J. Blum, *Numerical Simulation and Optimal Control in Plasma Physics: With Applications to Tokamaks*. Paris, France: Wiley, 1989.

[41] R. Goldston, "Energy confinement scaling in Tokamaks: Some implications of recent experiments with Ohmic and strong auxiliary heating," *Plasma Phys. Controlled Fusion*, vol. 30, no. 8, pp. 87–103, 1990.

[42] P. Politzer and G. Porter, "Power threshold for neutral beam current drive," *Nucl. Fusion*, vol. 30, no. 8, p. 1605, 1990.

[43] F. Argomedo, E. Witrant, and C. Prieur, "Input-to-state stability of a time-varying nonhomogeneous diffusive equation subject to boundary disturbances," in *Proc. Amer. Control Conf.*, 2012.

[44] H. K. Khalil, *Nonlinear Systems*, 3rd ed. Englewood Cliffs, NJ, USA: Prentice-Hall, 2002.

[45] J. Ferron, M. Walker, L. Lao, H. John, D. Humphreys, and J. Leuer, "Real time equilibrium reconstruction for tokamak discharge control," *Nucl. Fusion*, vol. 38, no. 7, p. 1055, 1998.

[46] D. Piglowski, J. Ferron, P. Gohil, R. Johnson, and B. Penaflor, "Enhancements in the second generation DIII-D digital plasma control system," *Fusion Eng. Des.*, vol. 82, nos. 5–14, p. 1058, 2007.
[47] M. Walker, J. R. Ferron, S. H. Hahn, D. A. Humphreys, Y. In, R. D. Johnson, *et al.*, "Advances in integrated plasma control on DIII-D," *Fusion Eng. Des.*, vol. 82, nos. 5–14, pp. 1051–1057, 2007.
[48] J. Barton, Y. Ou, C. Xu, E. Schuster, and M. Walker, "Simserver simulation of a model-based current profile controller in the DIII-D plasma control system," *Fusion Eng. Des.*, vol. 86, nos. 6–8, p. 1116, 2011.

Mark D. Boyer received the B.Sc. degree in mechanical engineering from York College of Pennsylvania, York, PA, USA, in 2009, and the Ph.D. degree in mechanical engineering from Lehigh University, Bethlehem, PA, USA, in 2013.

He is currently a Post-Doctoral Fellow with Princeton Plasma Physics Laboratory, Department of Energy Fusion Energy Sciences Post-Doctoral Research Program. His current research interests include the control of nonlinear and distributed parameter systems, with applications, including burn control and kinetic profile control in nuclear fusion reactors.

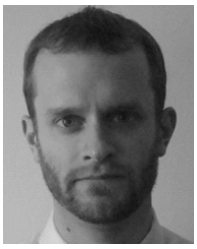

Justin Barton received the B.Sc. degree in mechanical engineering from Lehigh University, Bethlehem, PA, USA, in 2009, where he is currently pursuing the Ph.D. degree with the Department of Mechanical Engineering and Mechanics.

His current research interests include the control of distributed parameter and nonlinear systems with applications to plasma control in magnetic confinement fusion reactors.

Eugenio Schuster received the Undergraduate degrees in electronic engineering from Buenos Aires University, Buenos Aires, Argentina, in 1993, and in nuclear engineering from the Balseiro Institute, Río Negro, Argentina, in 1998, and the M.Sc. and Ph.D. degrees in mechanical and aerospace engineering from the University of California San Diego, San Diego, CA, USA, in 2000 and 2004, respectively.

He is an Associate Professor with the Department of Mechanical Engineering and Mechanics, Lehigh University, Bethlehem, PA, USA. He is the Director of the Laboratory for Control of Complex Physical Systems and the Head of the Lehigh University Plasma Control Group. He is involved in plasma control problems, including equilibrium control, burn control, magnetic and kinetic profile control, and MHD stabilization. His current research interests include distributed-parameter and nonlinear control of nuclear-fusion plasmas.

Prof. Schuster is a recipient of the National Science Foundation Career Award.

Michael L. Walker has been with the Energy Group of General Atomics, which operates the DIII-D tokamak under contract to the U.S. Department of Energy, since 1992. His principle area of responsibility is support of plasma control and operations. He has developed tokamak control algorithms from initial physics modeling through experimental model validation, control design using modern multivariable techniques, implementation in C and assembly language, and incorporation into daily operation of DIII-D and other tokamaks. He is the primary developer for the initial real time control algorithms in both EAST and KSTAR plasma control systems and participates regularly in operation of both tokamaks. He is currently the Principal Investigator for the General Atomics KSTAR collaboration. He actively supports international efforts to develop a conceptual plasma control system design for the control data access and communication system for the ITER tokamak, now under construction in southern France.

Tim C. Luce, photograph and biography not available at the time of publication.

John R. Ferron received the B.S. degree in physics from the University of Wisconsin, Madison, WI, USA, in 1974, and the Ph.D. degree from the University of California, Los Angeles, CA, USA, in 1982.

He is an Experimental Physicist with General Atomics, San Diego, CA, USA, involved in DIII-D tokamak. His research emphasis has been on high beta tokamak discharges and the effect of current and pressure profile shapes on stability and confinement. His current research interests include the development of steady-state advanced tokamak discharges utilizing off-axis neutral beam and electron cyclotron current drive in plasmas with a large fraction of self-driven bootstrap current.

Ben G. Penaflor, photograph and biography not available at the time of publication.

Robert D. Johnson, photograph and biography not available at the time of publication.

David A. Humphreys received the Ph.D. degree in plasma physics from the Massachusetts Institute of Technology, Cambridge, MA, USA, in 1990.

He is the Head of the DIII-D Plasma Control Group, General Atomics, San Diego, CA, USA. His 30 years of experience in fusion plasma physics and control have included engineering physics studies and magnetohydrodynamic analysis for many operating and next-generation tokamaks, including DIII-D, NSTX, JET, EAST, KSTAR, and ITER. His current research interests include MHD instabilities, model-based fusion plasma control, and tokamak disruptions.